RSC Advances

ROYAL SOCIETY OF CHEMISTRY

www.rsc.org/advances

Porous conducting polymer and reduced graphene oxide nanocomposites for room temperature gas detection

Yajie Yang*, Xiaojie Yang, Wenyao Yang, Shibin Li, Jianhua Xu, Yadong Jiang

State Key Laboratory of Electronic Thin Films and Integrated Devices, School of Optoelectronic Information, University of Electronic Science and Technology of China (UESTC), Chengdu 610054, P. R. China

We report chemical in situ deposition of porous conducting polymer poly(3,4-ethylenedioxythiophene) (PEDOT) on reduced graphene oxide (RGO) film as efficient chemiresistor sensor platform for room temperature NH_3 gas detection. Well covering of porous PEDOT on RGO was achieved through a simple baking treatment during the in situ polymerization of PEDOT. The well covering of porous PEDOT on RGO surface was confirmed by SEM, UV-Vis spectra, and FT-IR spectra methods. The gas sensing performance revealed that, in contrast to bare RGO and common PEDOT, the porous PEDOT/RGO based gas sensor exhibited an obvious sensitivity enhancement as well as response/recovery performance. The large surface area and highly opened structure of porous PEDOT resulted in excellent synergistic effect between PEDOT and RGO during the gas sensing process. As a result of the uniform distribution of PEDOT porous network onto RGO sheets, this nanocomposite based sensor also exhibited higher selectivity to NH_3 in contrast to other reductive analyte gases.

Introduction

* The corresponding author email: jj_eagle@163.com , Tel: +86-28-83208959 , Fax: +86-28-83206123

As one specific branch of graphene, the study of graphene oxide (GO) and GO-based materials has been popular and extensive recently.[1,2] Compared with pristine graphene, the covalent oxygenated functional groups in GO can indeed give rise to remarkable structure defects.[3] The presence of these functional groups also provide potential advantages for using GO in numerous applications.[4,5] These functional groups serve as sites for chemical modification or functionalization of GO, which in turn can be employed to immobilize various electroactive species through covalent or noncovalent bonds for the design of sensitive chemical and electrochemical systems.[6-10]

The ease of synthesis and solution processability has made GO a very attractive material for nanocomposite and graphene-related electronics applications.[11-16] By controlling the structural disorder, GO can be made into an insulating, semiconducting, or semimetallic material by appropriately fine-tuning the oxidation or reduction parameters.[17-20] As a reduction product of GO, reduced graphene oxide (RGO) resembles graphene but with some residual oxygen and structural defects, yielding a conductivity that is comparable to that of doped conductive polymers.[21,22] So, the composites based on RGO and conducting polymer shows good synergetic effects to improve performance.[23-25] The tunable electrical performance of RGO also makes it as promising functional materials.[26-28] The improved conductive performance and defective nature of RGO indicate very different chemical reactivity compared to graphene and GO.[29-32] Recently, RGO has been aroused much attention for using as chemiresistor based gas sensors, due to its scalable production, solution processability, large available surface area, etc.[33,34] Although above works reported the sensing properties of RGO, it is still a great

challenge to develop the sensing devices based on RGO for improved sensitivity and selectivity.

Conducting polymer and its nanostructure, as an excellent sensing material, has been extensively studied because of its high sensitivities, excellent reliability, and low cost properties.[35-37] Hybridization of conducting polymer with GO and RGO has been studied and the enhancement of sensitivity and selectivity of gas sensor compared with pure GO and RGO sensors was reported.[38,39] It has been demonstrated that conducting polymer, especially the nanostructured conducting polymer, plays important roles in enhancement of the sensing performance of GO and RGO devices.[40,41] However, there is no report about RGO and porous conducting polymer nanostructures for room temperature gas detecting. It is expected that the decoration of a porous conducting polymer nanostructure on the surface of RGO can greatly improve the sensitivity and selectivity of the pure RGO based sensor, through the combination of both excellent sensing materials. Therefore, we demonstrate, a NH_3 gas sensor based on RGO and porous conducting polymer poly(3,4-ethylenedioxythiophene) (PEDOT) nanostructure. The RGO layer is obtained from the GO Langmuir-Blodgett deposition and a subsequent thermal reductive treatment. The porous PEDOT nanostructure has been successfully deposited on the surface of RGO sheets by using a baking treatment during the in situ polymerization of 3,4-ethylenedioxythiophene (EDOT) monomer. The resultant porous PEDOT/RGO nanocomposite has been studied as excellent sensing materials for the detection of NH_3 gas at room temperature.

Results and discussion

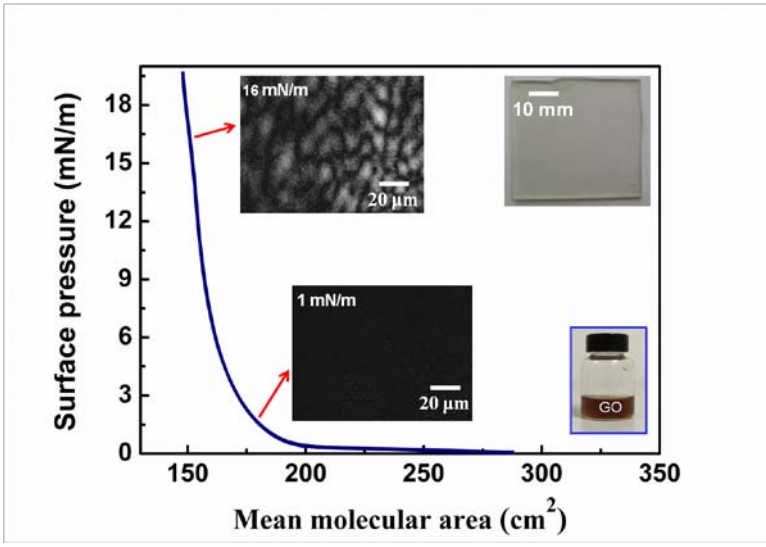

Fig. 1 surface pressure-mean molecular area (π-A) isotherm curves and BAM images of GO at different surface pressure (the inset pictures show a GO dispersion solution for LB deposition and RGO LB film covered ITO).

Fig. 1 show the surface pressure-area (π-A) curve of GO sheets at air-water interface and GO BAM images at different surface pressure. The results indicate that GO sheets can arrange closely at air-water interface with continuous compression to high surface pressure. These compact GO sheets at air-water interface can be deposited on different substrate, such as ITO and SiO_2, through vertical or horizontal LB deposition. The right inset pictures in Fig. 1 shows the GO water dispersion for LB deposition and a RGO LB film covered ITO. The RGO LB film shows obvious advantages for the transparency electrode material applications.

Fig. 2(a) shows AFM images of GO LB sheets deposited on substrate. It can be seen that highly compact arrangement of GO sheets are obtained through the LB deposition. The slight overlapping of GO sheets is observed (as shown by arrow in Fig. 2(a),(b)), and we deduce this results from the overlapping of sheets during the compressing of GO sheets at air-water interface. This LB deposition results in a 1-1.2 nm thickness ultrathin

GO layer with highly compact formation. By controlling the surface pressure, large area GO sheets with continuous formation can be also deposited on substrates. We intend to introduce this large area and formation tunable GO layer to obtain RGO layer after a reductive treatment, and a porous conducting polymer can be constructed on latter formed RGO layer as novel nanocomposites.

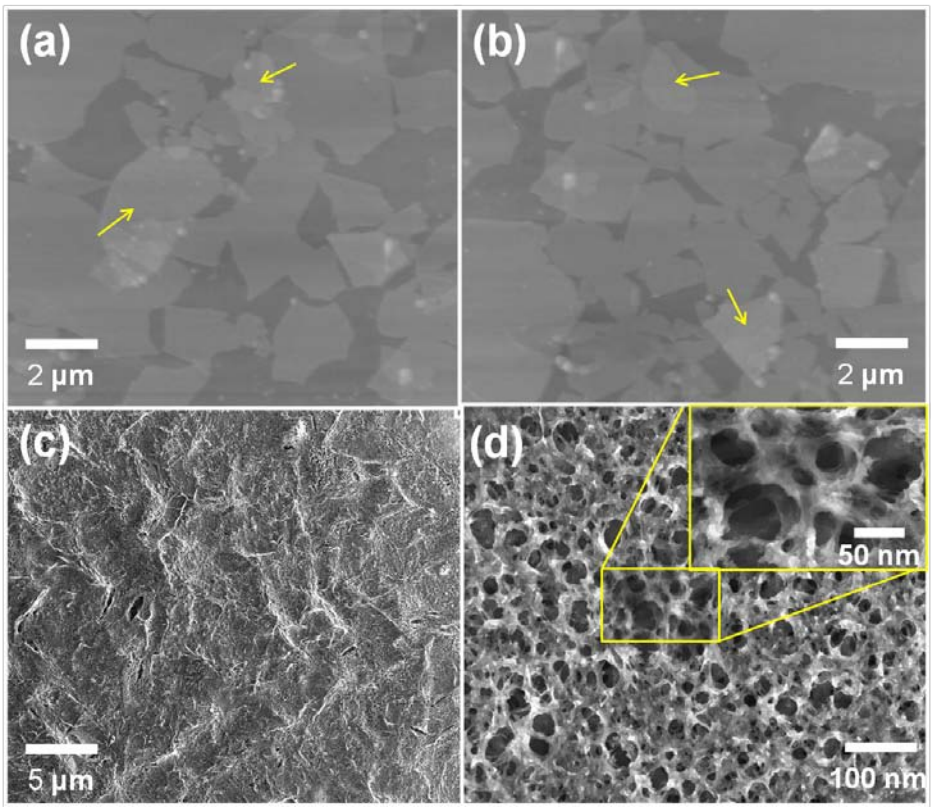

Fig. 2 AFM images of (a) GO and (b) RGO LB films, and (c), (d) SEM images of porous PEDOT layer deposited on RGO LB films.

We choose a thermal treatment at water vapor environment as efficiently reduction process to obtain RGO sheets.[32] After the thermal reductive treatment, compared with as-prepared GO layer, the obtained RGO sheets keep the ordered and compact formation (as shown in Fig. 2(b)). The results in Fig. 2 indicate that the excellent covering performance of RGO LB layer can bridge a large scale and continuous sheets

as sensing materials.

After the thermal reduction of GO sheets, a porous PEDOT nanostructure was constructed on RGO through the combination of in situ polymerization and a simple speedy baking method. The RGO covered substrate was dipped into and out slowly from the PEDOT solution, and this slow dip-coating process produces a wet PEDOT layer containing solvent on RGO. Then, this wet PEDOT layer is quickly transferred into a vacuum oven, and a speedy baking process is utilized to form the porous PEDOT nanostructure due to the fast volatilizing of solvent from inside PEDOT layer. Fig. 2(c) shows SEM image of porous PEDOT layer deposited on RGO layer after the baking process. The surface of PEDOT layer exhibits slightly fluctuate morphology after in situ dip-coating deposition. Fig. 2(d) shows a larger magnification SEM image of porous PEDOT deposited on RGO. The uniform and well distribution of hole nanostructure in PEDOT layer is presented. In our experiment, a mixed solvent containing n-butyl alcohol and acetone is utilized as solution for in situ polymerization of EDOT monomer. The n-butyl alcohol can form stable PEDOT solution and the acetone with low boiling point makes sure the controllable solvent volatilizing from inside PEDOT layer during the baking process. The fast volatilizing of solvent has resulted in a bubble-like volatilization process, leading to a porous PEDOT nanostructure. Then, by controlling the speed of baking, a uniformly porous PEDOT nanostructure can be obtained on RGO surface.

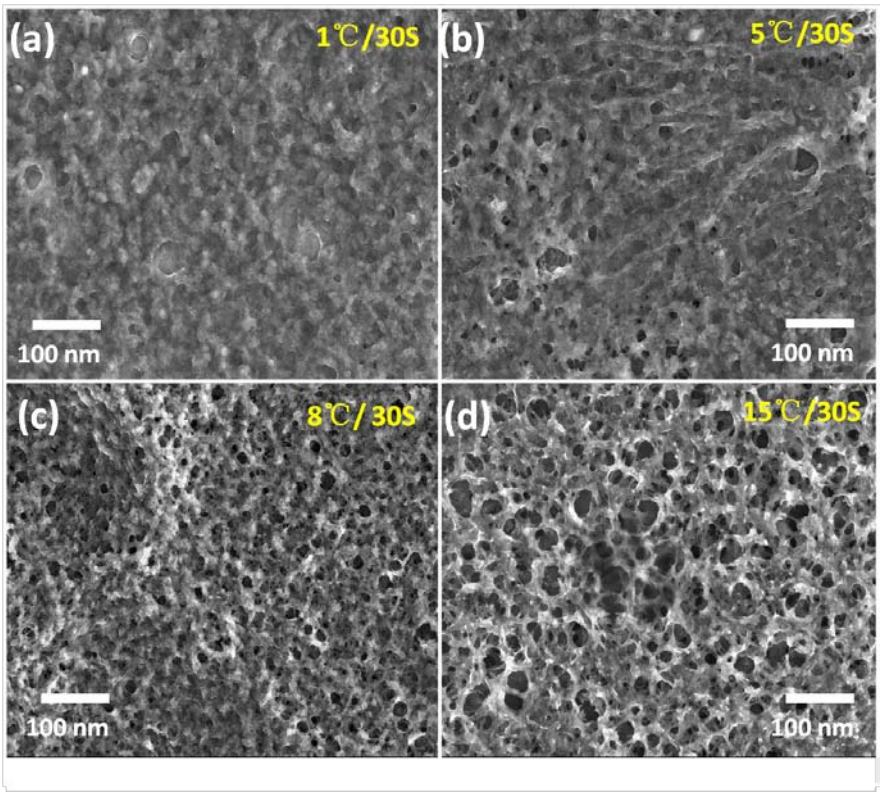

Fig. 3 Influence of heating rates during baking process on porous structure of obtained PEDOT layer on RGO.

As exhibited in Fig. 3, a speedy baking results in more uniform porous structure of PEDOT nanostructures. At slower heating rates (1-5 ℃/30 sec), the obtained PEDOT layer exhibits a compact film morphology due to the slow volatilization of solvent. In this baking process, we confirmed that no distinct bubble-like volatilization occurred due to the slow volatilization of solvent from inside PEDOT. At the faster heating rates (8-15℃/30 sec), the well controlled and fast volatilizing of solvent leads to the solvent molecules diffusing fast from the inside PEDOT layer with a bubble-like formation, and the baked PEDOT layer exhibits obviously porous structure. It also can be found that this composite exhibits a continuous PEDOT network structure as continuous sensing layer

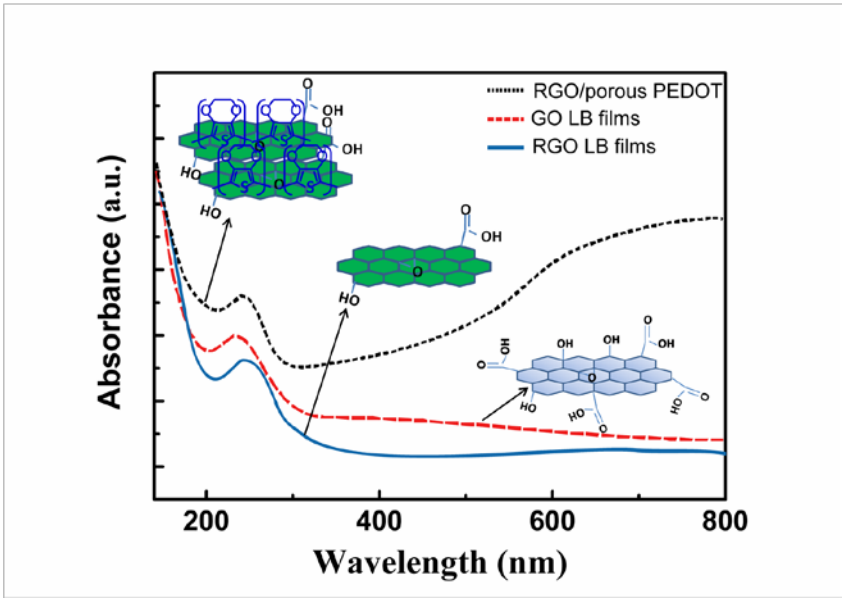

Fig. 4 UV-Vis spectra of GO LB film, RGO LB film and RGO/porous PEDOT.

The process for the preparation of GO, RGO LB film and RGO/porous PEDOT was monitored by UV-Vis spectroscopy (Fig. 4). The GO LB film shows the absorption peak at 258 nm, and slightly red-shift is observed after the thermal treatment due to the reduction of GO into RGO. This result also confirms the successful reduction of GO into RGO after the thermal treatment, leading to the optical and conductive characteristics change of GO. After the deposition of porous PEDOT on RGO sheets, the appearance of a wide absorption peak from 600 nm to 800 nm derives from the polarons and bipolarons due to partly doping of p-toluene sulfonate hexahydrate (PTS^-) into PEDOT backbone. This result confirms that the porous PEDOT has been successfully deposited on RGO LB layer through in situ chemical polymerization. Due to the construction of a porous PEDOT structure on the RGO surface, the UV-Vis spectrum of composites also exhibits a 258 nm peak.

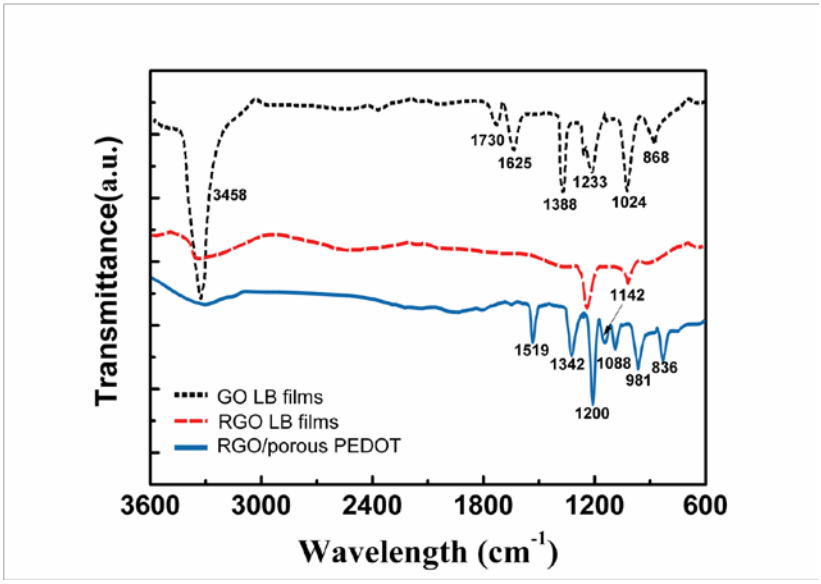

Fig. 5 FT-IR spectra of GO LB film, RGO LB film and RGO/porous PEDOT.

The FT-IR spectra of GO, RGO LB film and RGO/porous PEDOT are shown in Fig. 5. The peaks locate at 3458 cm^{-1} and 1388 cm^{-1}, corresponding to the O–H stretching and vibration mode of intercalated water. The characteristic peaks of oxygen moieties locate at 1233 cm^{-1}, 1625 cm^{-1} and 1730 cm^{-1}, corresponding to C–O (n(epoxy or alkoxy)), C–O in carboxylic acid, and carbonyl moieties (n(carbonyl), respectively.[42] The FT-IR spectra of RGO indicates that the thermal reduction of GO at the water vapor environment is relatively complete with few oxygen-containing groups. From the FT-IR spectrum of RGO/porous PEDOT, the vibrational bands at about 1,519 cm^{-1} and 1,342 cm^{-1} are attributed to the C=C and C–C stretching vibrations of the quininoid structure of the thiophene ring, respectively. The bands at 1,200 cm^{-1}, 1,142 cm^{-1}, and 1,088 cm^{-1} are ascribed to the C–O–C bond stretching in the ethylene dioxy (alkylenedioxy) group. Additionally, the C–S bond in the thiophene ring is demonstrated by the presence of bands at about 981 cm^{-1} and 836 cm^{-1}. The series of bands suggests that the PEDOT is deposited on RGO through an in situ polymerization deposition.[43]

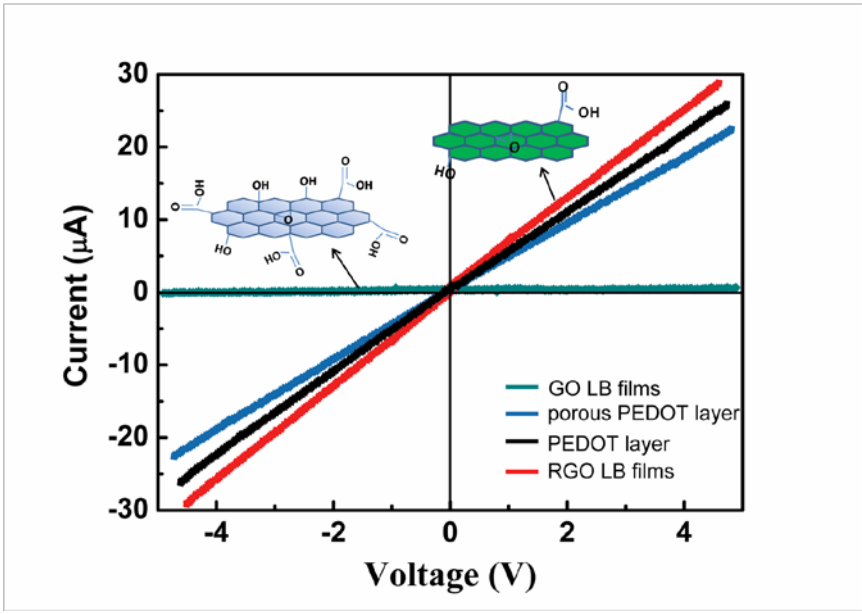

Fig. 6 Current versus voltage (I-V) performance of GO LB film, RGO LB film, common PEDOT and porous PEDOT.

The excellent covering performance of GO LB films results in continuous and effect covering of active layer after the thermal reduction. The thermal treatment at water vapor environment results in the reduction of GO into RGO efficiently, accompanying with structure and conductivity change of GO. The better conductivity of RGO assures good ohmic contact between sensing layer and electrodes. The I-V curves of GO, RGO LB films and porous PEDOT shown in Fig. 6 indicate that an obvious enhancement of RGO conductivity is obtained after the thermal treatment of GO. It is well known that the RGO exhibits tunable electrical performance depending on the reduction level of GO, and this is also a useful property for the application in sensing applications.[32] As shown in Fig. 6, porous PEDOT shows lower conductivity than RGO and common PEDOT, but exhibit compared conducting performance with both two. The highly reductive GO presents a conductivity that is comparable to doped conductive polymers due to some residual oxygen and structural defects.[2] The comparable electrical

performance between RGO and porous PEDOT also makes sure good synergistic effect in composites and lower noise response of gas sensor. As for relative lower conductivity of porous PEDOT/RGO, we deduced that the complicated deposition process may cause a non-uniform PEDOT structure on RGO, especially on the surface of RGO, resulting in some negative influence on conducting performance of porous PEDOT/RGO.

The gas sensitivity of porous PEDOT/RGO based sensors to NH_3 was measured according to the resistance change of device after the exposure of sensor to analyte gases and the resistance variations of device were monitored. Based on the LB and dip-coating methods, the porous PEDOT/RGO is deposited on the interdigitated electrode accordingly, and the continuous sensing layer was constructed across the electrode to form effective sensing layer. The inset picture in Fig. 8(a) shows the SEM image of interdigitated electrode covered by porous PEDOT/RGO composites. Obviously, the porous PEDOT/RGO is bridging the gaps of electrodes, and effective sensing layer is constructed across the electrode arrays.

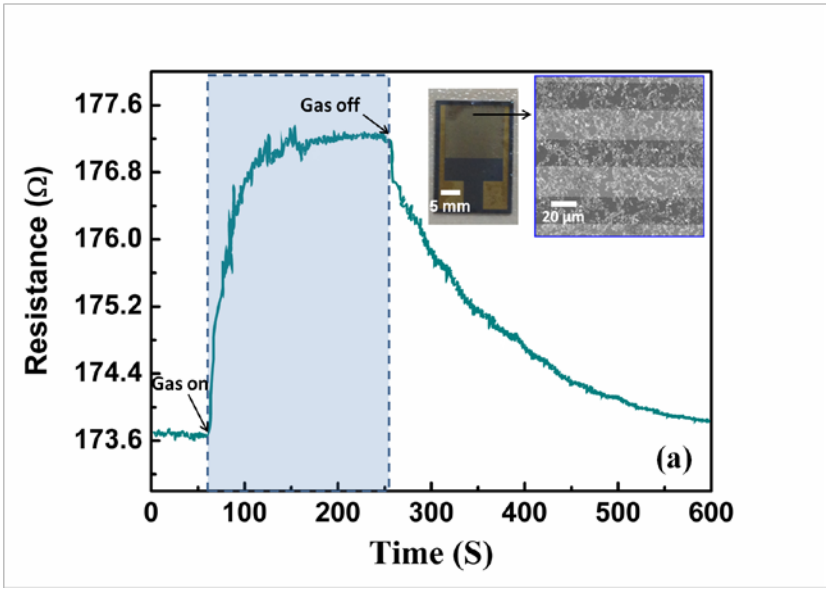

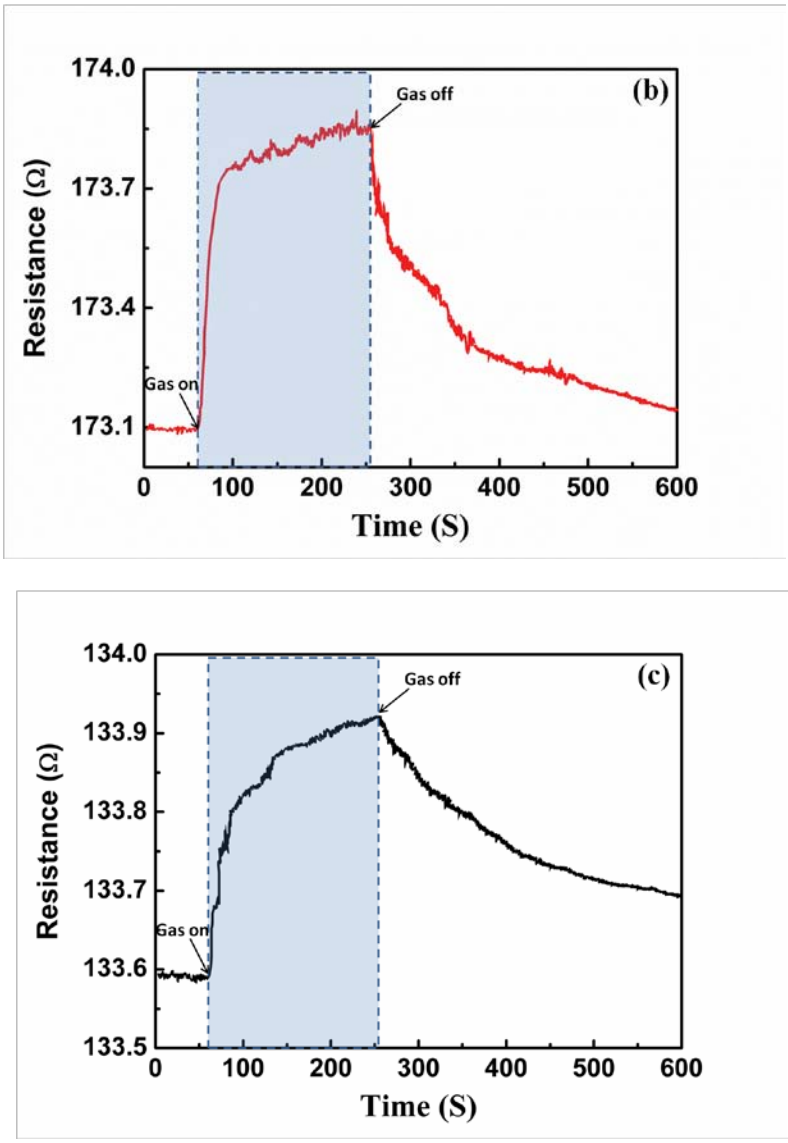

Fig. 7 Gas sensitivity of sensor with (a) porous PEDOT/RGO, (b) bare RGO and (c) common PEDOT as sensing layers to 5 ppm NH_3, and the inset picture in (a) are SEM image and photo picture of porous PEDOT/RGO covered interdigitated electrode.

Fig. 7 displays the comparison of the response of the resultant sensor based on bare RGO, common PEDOT and porous PEDOT/RGO toward 5 ppm NH_3 gas. As the NH_3 gas was released to the chamber, the resistances of all devices increase. The exposure of the device based on the porous PEDOT/RGO to NH_3 gas results in an ohm level change of the resistance, which exhibits an obvious sensitivity enhancement to NH_3 gas than

bare RGO and common PEDOT based devices. This result suggests that a porous nanostructure constructed on RGO obviously improves the gas sensitivity of devices. This porous PEDOT/RGO based sensor exhibits a 90-100 S response time and less than 180 S recovery time to 5 ppm NH_3 gas. Compared with bare RGO, the improvement of surface area supplying by porous PEDOT can be of benefit for the enhancement adsorption of NH_3 gas, resulting in a much better and enhancement of sensing performance. The obvious enhancement of sensitivity also suggested that the gas sensing synergetic effects have occurred between porous PEDOT and RGO sheets, leading to a great improvement of the sensing performance.

As shown in Fig. 7(a) and (b), both porous PEDOT/RGO and bare RGO sensors show fast response and recovery performance, indicating that both the bare RGO and composite supply highly opened surface area for fast adsorption and complete desorption of NH_3 gas.[29,30] However, the bare RGO based sensor exhibits less resistance change and less sensitivity. For common PEDOT sensing layer, lowest resistance change was observed. We conclude that the nonporous structure of common PEDOT sensing layer results in the long period of adsorption and desorption of analyte gas during the sensing process. Almost complete recovery to initial resistance of the devices are achieved for the sensing device based on porous PEDOT/RGO and bare RGO during the desorption process. Due to the high surface ratio of RGO sheets and porous PEDOT nanostructure, fast response is presented for the sensing device based on this composite. In contrast to the bare RGO and common PEDOT, the porous PEDOT/RGO can not only supply a porous conducting polymer structure with large surface area for

improved gas sensitivity, the porous structure also supply preferred surface formation for adsorption and desorption of gas molecules.

We investigated the impact of porous morphology in PEDOT on gas sensing performance of porous PEDOT/RGO based gas sensors, which is shown in Fig. 8. It is obvious that the sensor based on porous PEDOT/RGO composites obtained at 15 ℃ /30S baking speed exhibits best sensing performance. This porous PEDOT/RGO sensing layer contains larger size holes and the uniform hole distribution. During the long time exposure of sensor to 5 ppm NH_3 gas, this device shows fast response and recovers to initial state rapidly after the cutting off the analyte gas. It is convinced that the uniform distribution of porous structures in PEDOT tremendously improves the adsorption amounts of gas molecules during the sensing process, and the highly opened surface also results in excellent recovery performance of gas sensors.

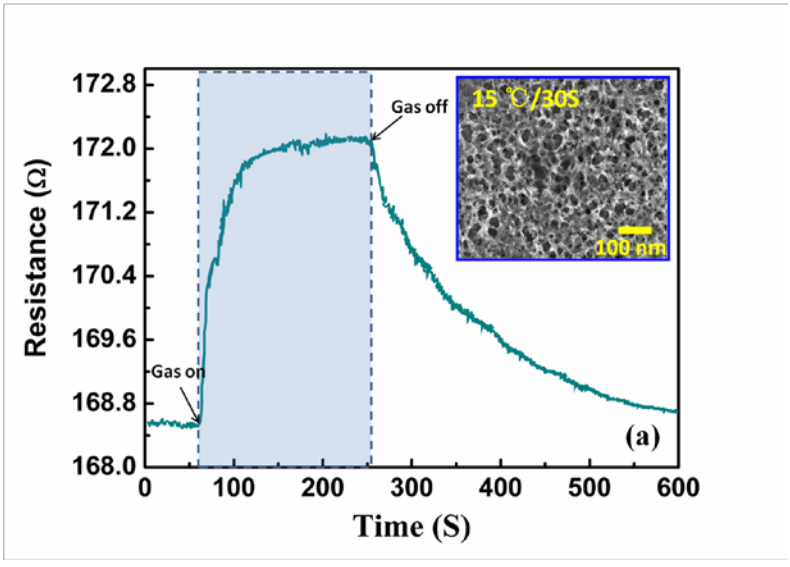

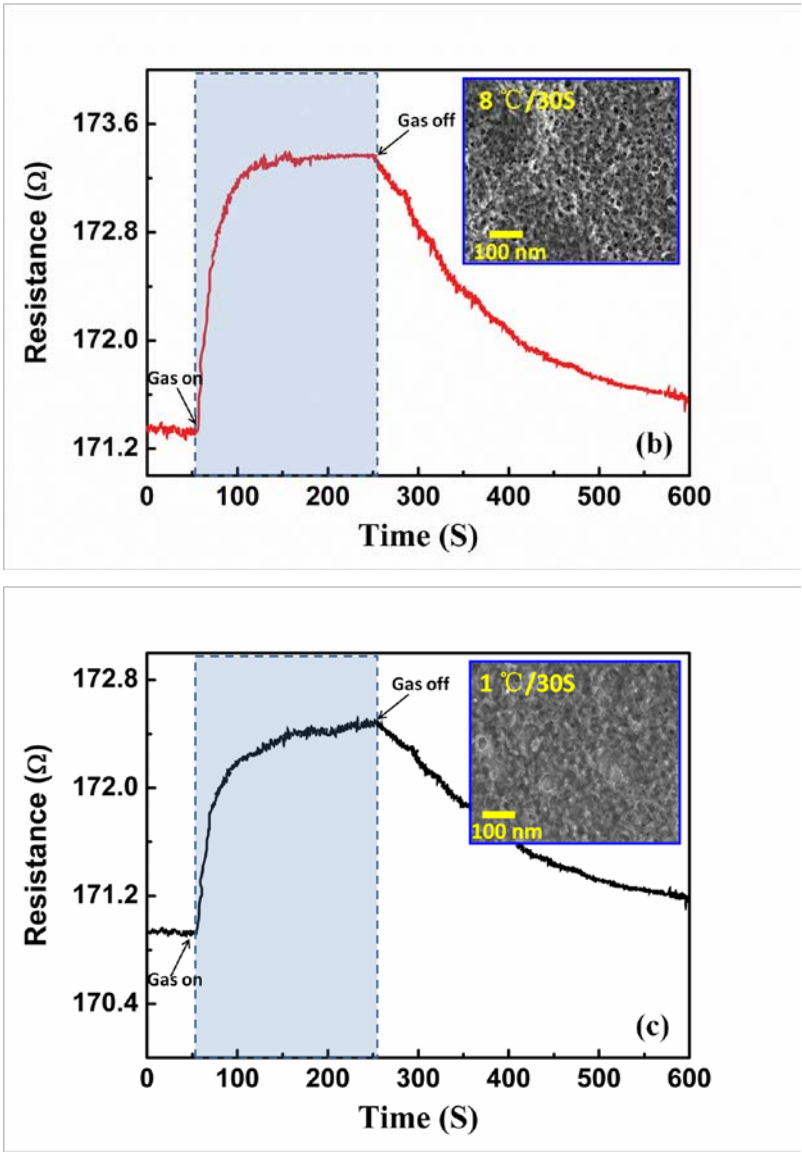

Fig. 8 Influence of porous PEDOT structure obtained from different baking speed (a) 15℃/30S, (b) 8℃/30S and 1℃/30S on gas sensitivity of sensor to 5 ppm NH_3.

The reproducibility of porous PEDOT/RGO based gas sensor is shown in Fig. 9. It can be seen that the sensor exhibits excellent repeatable characteristic, and the response levels of the sensor can be maintained after repeated cycles of exposure to NH_3 and recovery. It is suggested that the excellent sensing properties of porous PEDOT/RGO based sensors are governed by the intrinsic properties of RGO as well as porous PEDOT. RGO sheets still have parts of oxygen-based moieties and structure defects

after thermal reduction process, which can generally lead to the p-type semiconducting behavior of the resultant RGO.[45] NH_3, as a reducing agent, has a lone electron pair that can be easily donated to the p-type RGO sheets, leading to the increase of the resistance of the RGO based devices. As for conducting polymer PEDOT, the exposure of porous PEDOT to NH_3 also increase the resistance of composite due to the dedoping of PEDOT. Compared with bare RGO or common PEDOT, the accumulation of resistance change caused by RGO and porous PEDOT spontaneously results in the enhancement of sensitivity of composites based gas sensor. Moreover, as typical π electronic systems, PEDOT can interact with RGO sheets through the Pi–Pi interaction at the interface of RGO and porous PEDOT. This Pi–Pi interaction between PEDOT and RGO sheets is also attributed to the sensitivity enhancement of composite based gas sensor.[44]

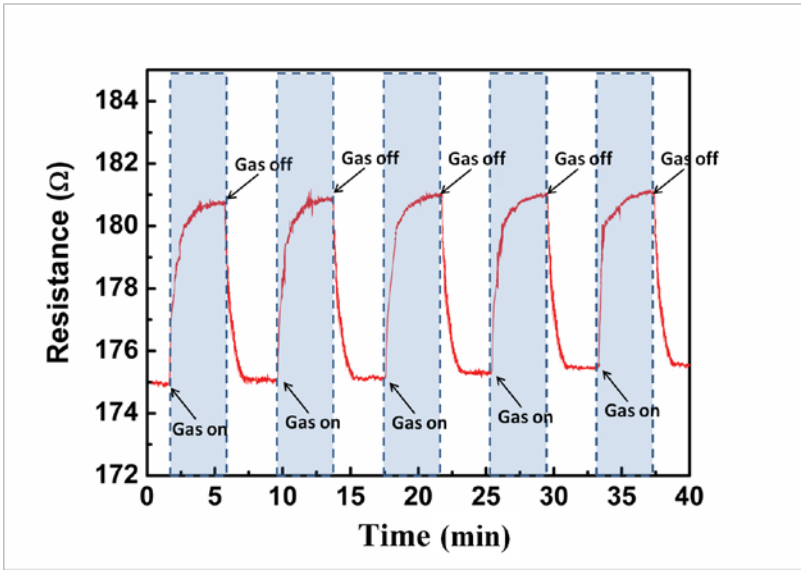

Fig. 9 Repeatable characteristic of RGO/porous PEDOT based sensor to 5 ppm NH_3 gas.

Fig. 10 shows the response of the sensor based on porous PEDOT/RGO to different concentrations of NH_3 gases at room temperature. During the exposure of the device to

different concentrations NH_3 gas, the obvious resistance change can be achieved for the case of gas concentration from 10 ppm to 200 ppb. The results indicate that, even at ppb level, the porous PEDOT/RGO based sensing device exhibits a fast response and recovery performance. With the increasing of NH_3 gas concentration, the resistance of the device increases accordingly. This result indicates that the porous PEDOT/RGO nanostrucrure based gas sensors shows promising application as candidate for actual NH_3 gas detection in atmosphere condition.

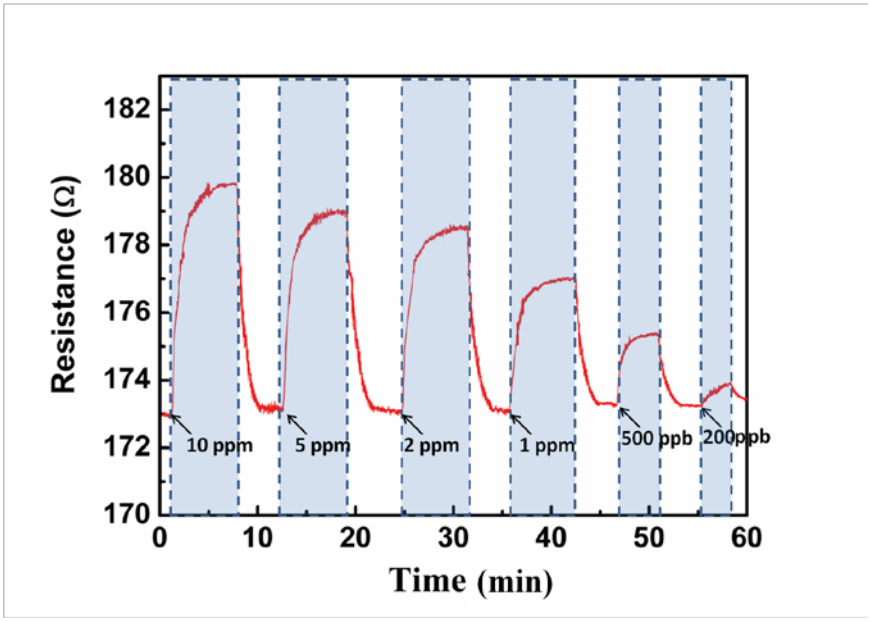

Fig. 10 Sensitivity of porous PEDOT/RGO based sensor to different concentration NH_3 gas.

As we discussed above, gas sensor based on bare RGO and common PEDOT exhibit inferior sensitivity to NH_3. The inferior performance of common PEDOT based sensor is attributed to the direct deposition of compact PEDOT as sensing layer. This common and compact conducting polymer layer did not afford highly opening surface area for fast adsorption and deposition. The fast speed baking process produces uniform distribution of porous structure in PEDOT layer, leading to a more opening surface area

for gas molecules adsorption. It has been found in our work the porous PEDOT layer contains surface area about 20 m^2g^{-1}, which is compared with PEDOT nanoparticle (average diameter 50 nm) surface area about 29 m^2g^{-1}. So, compared with common PEDOT layer, the porous PEDOT structure affords highly opening surface area for gas molecules adsorption during sensing process. The large and opening surface of porous structure contributes to fast adsorption and desorption of NH_3 molecules for enhanced sensitivity.

As promising gas sensing materials, bare RGO affords the high surface area and low noise response for gas detection. But the high selectivity of bare RGO based gas sensor is still a challenge for low concentration gas detection. So, we investigate the selectivity of this porous PEDOT/RGO based sensor. The sensor response toward different gases was calculated according to the following equation:

$$R(\%)=\Delta R/R_e\times100=(R_b-R_c)\times100/R_e$$

In this equation: the R_b and R_c are the resistance of porous PEDOT/RGO composite before and after exposure to different gases respectively.

As shown in Fig. 11, NH_3 gas has been used for the evaluation of the sensor through the comparison with other different analyte gases, e.g., SO_2, CH_2Cl_2, CH_3OH, in same concentration. The porous PEDOT/RGO gas senor shows obviously high selectivity to 1 ppm NH_3 compared with other analyte gases. The high selectivity of porous PEDOT /RGO based gas sensor demonstrates that this composite is an excellent candidate for the detection of NH_3 gas in complex gases. In Fig. 11, the sensing performance of the sensor based on porous PEDOT/RGO has been also compared to that of gas sensor

based on bare RGO. The gas sensor based on the porous PEDOT/RGO exhibits much higher response than that of the gas sensor based on bare RGO. The construction of porous PEDOT nanostructure on RGO layer has tremendously increased the sensing selectivity of gas sensor to low concentration NH_3 gas. Moreover, we deduced that Pi–Pi interaction between PEDOT and RGO sheets is also attributed to this selectivity enhancement of composite based sensor to HN_3.[44] As for other gas analytes, the better sensitivity is also achieved compared with pure RGO based gas sensor. For oxidant gas of H_2S and SO_2, the porous PEDOT/RGO gas sensor show reverse trend compared to other analyte gases. This reverse trend sensitivity is ascribed to the doping of composite after the exposure of H_2S and SO_2, leading to the improved conducting performance of composite.

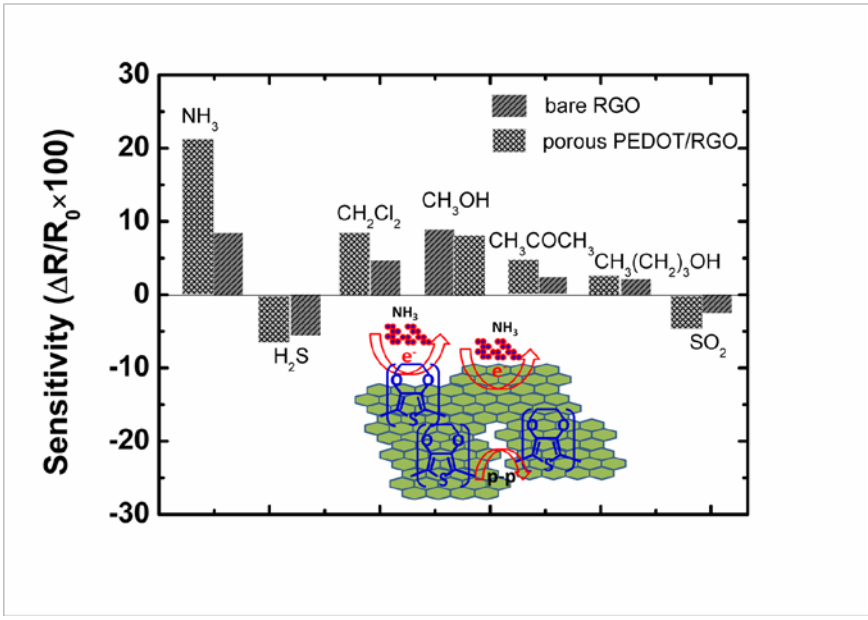

Fig. 11 Gas selectivity of bare RGO and porous PEDOT/RGO based device to 1 ppm different analyte gases.

Conclusion

A porous PEDOT/RGO nanocomposite has been successfully prepared by LB

deposition and in situ polymerization method. The porous PEDOT nanostructure is constructed on RGO LB films through a speedy baking during the in situ solution polymerization of EDOT. The high surface area and porous nanostructure of this novel nanocomposite enhance gas adsorption and desorption. The results of gas sensing performance indicates that the RGO/porous PEDOT composite based device exhibits excellent sensing performance to NH_3 gas compared with those of the sensors based on bare RGO and common PEDOT. The porous nanostructure of conducting polymer PEDOT constructed on RGO shows promising application for high performance gas sensors due to the tremendous enhancement of sensitivity and selectivity of gas sensor to ppb level detection of toxic NH_3 gas.

Experimental Section

Instruments: The surface pressure–area (π–A) isotherm recorded by computer and the morphology analysis of GO sheets at air–water interface was characterized by the BAM 300 Brewster Angle Microscopy. Surface morphology of GO and RGO film were investigated by SP 3800 atomic force microscopy (AFM) with a tapping mode. UV-Vis spectrum of the film was recorded on a UV 1700 spectrometer. FT-IR spectrum was characterized with an ALPHA analysis instrument. The Morphological properties of porous PEDOT/RGO were investigated with a Hitachi S-2400 scanning electron microscopy (SEM). The current–voltage (I−V) curve was obtained by using a Keithley 4200 semiconducting testing system.

Materials. GO was synthesized from natural graphite flakes through Hummer's method. Graphite flakes used for GO preparation was purchased from Sigma-Aldrich. At first,

stable dispersion of GO in a solution mixture of methanol/deionized water (DI water) (4:1) was subjected to ultrasonication for 30 min followed by centrifugation at 2500 rpm. This as-prepared GO solution was used as LB film deposition. EDOT monomer and oxidizer Iron(III) p-toluene sulfonate hexahydrate (($Fe(PTS)_3$) for chemical in situ polymerization were purchased from Bayer Company and used as received. All solvents used in experiment are high purity level.

GO film deposition and reduction. A KSV-5000 LB system was used to obtain highly compact and single layer GO sheets. The trough was carefully cleaned with chloroform and then filled with DI water. GO solution was dropwise spread onto the water surface using a glass syringe. Surface pressure was monitored using a tensiometer attached to a Wilhelmy plate. The film was compressed by barriers at a speed of 1mm/min. The GO monolayer was transferred to substrates at various points during the compression by vertically dipping the substrate into the trough and slowly pulling it up (1 mm/min). The SiO_2 substrate for LB film deposition was first ultrasonicated in DI water for 30 min, and followed by a ultrasonicate treatment in Dimethylcarbinol for 15 min. This hydrophilic treatment can keep uniform coverage of GO sheets on substrate. After the LB deposition of GO on substrate, the sheets covered substrate was treated in a water vapor oven at 180 ℃ for 4 h reduction.[32]

Preparation of porous PEDOT on RGO. In situ polymerization solution of PEDOT was prepared by introducing 4.5 mL EDOT into 50 mL n-butyl alcohol and acetone mixed solution (volume ratio 1:1). After a thorough stirring, then 1.5 ml of $Fe(PTS)_3$ was introduced into the EDOT solvent mixture in order to trigger the polymerization of

EDOT. This in situ polymerization solution was kept at 5 °C for lower speed polymerization. Then, the RGO covered substrate was immersed into PEDOT solution by dip-coating process for an in situ deposition of PEDOT layer. This process was carried out in a KSV dip-coater with a drop in and out process to form ultrathin PEDOT layer. In order to obtain the uniform PEDOT layer for sensing performance comparison, the PEDOT layers with 80-110 nm thickness were formed on RGO at 0.5 m/min dipping speed. This wet PEDOT layer contained residential solvent of n-butyl alcohol and acetone. Then, the RGO/PEDOT covered substrate was quickly transferred into a vacuum oven for a speedy baking treatment. The oven temperature increased from room temperature to 80 °C with a 15 °C/30 sec heating rate, and the substrate was kept in 80 °C oven for 30 min. After the baking process of PEDOT for 30 min, the product was washed by ethanol to remove residual reagent.

Electrical and sensing performance testing. In order to investigate gas sensing performance of composites, a chemiresistor gas sensor device was used as detective platform. A conventional photolithographic method was used to fabricate the interdigitated electrode with a finger width of 30 μm and a gap size of 20 μm. The electrodes (30-nm Ti and 50-nm Au) were thermally evaporated on a layer of silicon dioxide (SiO_2). The RGO/PEDOT film was prepared across an interdigitated electrode (30 μm width) and tested in an airtight chamber. Prior to the measurement, the interdigitated electrode was blown with dry N_2 flow and corresponding vapor was injected into gas chamber. The resistance was monitored continuously over time. For selectivity test, the mixed gases were injected into gas chamber through a home-made

gas distribution system. The analytic gases with different concentrations were generated by mixing saturated vapors with dry air controlled by mass flow controllers. The resistance change of sensor was monitored with a computer controlled source meter (Keithley 2400). All the measurements were performed at ambient temperature.

Acknowledgements

This work was supported by the National Science Foundation of China (NSFC) (No.61101029 and 61371046)，a plan funding for supporting the New Century Talents (No. NCET-12-0091).

Notes and references

(1) Zhu Y. W.; Murali S.; Cai W. W.; Li X. S.; Suk J. W.; Potts J. R.; Ruof R. S. *Adv. Mater*. 2010, **22**, 3906.

(2) Dreyer D. R.; Park S.; Bielawski C. W.; Ruoff R. S. *Chem. Soc. Rev*. 2010, **39**, 228.

(3) Wan X. J.; Huang Y.; Chen Y. S. *Acc. Chem. Res*. 2012, **45**, 598.

(4) Chen D.; Feng H. B.; Li J. H. *Chem. Rev*. 2012, **112**, 6027.

(5) Compton O. C.; Nguyen S. T. *Small* 2010, **6**, 711.

(6) Zhou M.; Zhai Y. M.; Dong S. J. *Anal. Chem*. 2009, **81**, 5603.

(7) Eda G.; Chhowalla M. *Adv. Mater*. 2010, **22**, 2392.

(8) Zhang L. M.; Xia J. G.; Zhao Q. H.; Liu L. W.; Zhang Z. J. *Small* 2010, **6**, 537.

(9) Yang X. Y.; Zhang X. Y.; Liu Z. F.; Ma Y. F.; Huang Y.; Chen Y. S. *J. Phys. Chem. C* 2008, **112**, 17554.

(10) Robinson J. T.; Perkins F. K.; Snow E. S.; Wei Z. Q.; Sheehan P. E. *Nano Lett*. 2008, **8**, 3137.

(11) Dikin D. A.; Stankovich S.; Zimney E. J.; Piner R. D.; Dommett G. H. B.; Evmenenko G.; Nguyen S.T.; Ruoff R. S. *Nature* 2007, **448**, 457.

(12) Shen J. F.; Hu Y. Z.; Shi M.; Lu X.; Qin C.; Li C.; Ye M. X. *Chem. Mater.* 2009, **21**, 3514.

(13) Stankovich S.; Dikin D. A.; Piner R. D.; Kohlhaas K. A.; Kleinhammes A.; Jia Y. Y.; Wu Y.; Nguyen S. T.; Ruoff R. S. *Carbon* 2007, **45**, 1558.

(14) Kuilla T.; Bhadra S.; Yao D.; Kim N. H.; Bose S.; Lee J. H. *Prog. Polym. Sci*. 2010, **35**, 1350.

(15) Cote L. J.; Cruz-Silva R.; Huang J. X. *J. Am. Chem. Soc*. 2009, **131**, 11027.

(16) Zhu X. J.; Zhu Y. W.; Murali S.; Stoller M. D.; Ruoff R. S. *ACS Nano* 2011, **5**, 3333.

(17) Gómez-Navarro C.; Weitz R. T.; Bittner A. M.; Scolari M.; Mews A.; Burghard M.; Kern K. *Nano Lett*. 2007, **7**, 3499.

(18) Jung I.; Dikin D. A.; Piner R. D.; Ruoff R. S. *Nano Lett.* 2008, **8**, 4283.

(19) Pei S. F.; Cheng H. M. *Carbon* 2012, **50**, 3210.

(20) Kim F.; Cote L. J.; Huang J. X. *Adv. Mater*. 2010, **22**, 1954.

(21) Zhang J. L.; Yang H. J.; Shen G. X.; Cheng P.; Zhang J. Y.; Guo S. W. *Chem. Commun*. 2010, **46**, 1112.

(22) Wei Z. Q.; Wang D. B.; Kim S.; Kim S. Y.; Hu Y. K.; Yakes M. K.; Laracuente A. R.; Dai Z. T.; Marder S. R.; Berger C.; King W. P.; de Heer W. A.; Sheehan P. E.; Riedo E. *Science* 2010, **328**, 1373.

(23) Zhang J. T.; Zhao X. S. *J. Phys. Chem. C* 2012, **116**, 5420.

(24) Zhang L. L.; Zhao S. Y.; Tian X. N.; Zhao X. S. *Langmuir* 2010, **26**, 17624.

(25) Wang D. W.; Li F.; Zhao J. P.; Ren W. C.; Chen Z. G.; Tan J.; Wu Z. S.; Gentle I.; Lu G. Q.; Cheng H. M. *ACS Nano* 2009, **3**, 1745.

(26) Eda G.; Fanchini G.; Chhowalla M. *Nature Nanotech*. 2008, **3**, 270.

(27) Yin Z. Y.; Wu S. X.; Zhou X. Z.; Huang X.; Zhang Q. C.; Boey F.; Zhang H. *Small* 2010, **6**, 307.

(28) Fan W. F.; Lai Q. H.; Zhang Q. H.; Wang Y. *J. Phys. Chem. C* 2011, **115**, 10694.

(29) Lu G. H.; Ocola L. E.; Chen J. H. *Nanotechnology* 2009, **20**, 445502.

(30) Lu G. H.; Ocola L. E.; Chen J. H. *Appl. Phys. Lett*. 2009, **94**, 083111.

(31) Jeong H. Y.; Lee D. S.; Choi H. K.; Lee D. H.; Kim J. E.; Lee J. Y.; Lee W. J.; Kim S. O.; Choi S. Y. *Appl. Phys. Lett*. 2010, **96**, 213105.

(32) Han T. H.; Huang Y. K.; Tan A. T. L.; Dravid V. P.; Huang J. X. *J. Am. Chem. Soc*. 2011, **133**, 15264.

(33) Dua V.; Surwade S. P.; Ammu S.; Agnihotra S. R.; Jain S.; Roberts K. E.; Park S.; Ruoff R. S.; Manohar S. K. *Angew. Chem. Int. Ed*. 2010, **49**, 2154.

(34) Myers M.; Cooper J.; Pejcic B.; Baker M.; Raguse B.; Wieczorek L. *Sens. Actuators, B* 2011, **155**, 154.

(35) Bai H.; Shi G. Q. *Sensors* 2007, **7**, 267.

(36) Jang J.; Chang M.; Yoon H. *Adv. Mater*. 2005, **17**, 1616.

(37) Hatchett D. W.; Josowicz M. *Chem. Rev*. 2008, **108**, 746.

(38) Huang X. L.; Hu N. T.; Gao R. G.; Yu Y.; Wang Y. Y.; Yang Z.; Kong E. S. W.; Wei H.; Zhang Y. F. *J. Mater. Chem.* 2012, **22**, 22488.

(39) Basua S.; Bhattacharyya P. *Sens. Actuat. B* 2012, **173**, 1.

(40) Kuila T.; Bose S.; Mishra A. K.; Khanra P.; Kim N. H.; Lee J. H. *Prog. Mater. Sci*. 2012, **57**, 1061.

(41) Ratinac K. R.; Yang W. R.; Gooding J. J.; Thordarson P.; Braet F. *Electroanalysis* 2011, **23**, 803.

(42) Wang Y. J.; Liu J. C.; Liu L.; Sun D. D. *Nanoscale Res. Lett.* 2011, **6**, 241.

(43) Yang Y.J .; Jiang Y. D.; Xu J. H.; Yu J. S. *Polymer* 2007, **48**, 4459.

(44) Kang X. H.; Wang J.; Wu H.; Liu J.; Aksay I. A.; Lin Y. H. *Talanta* 2010, **81**, 754.

(45) Hua N. T.; Wang Y. Y.; Chai J.; Gao R. G.; Yang Z.; Kong E. S-W.; Zhang Y. F. *Sens. Actuators, B* 2012, **163**, 107.